Journal of Physics:
Conference Series

PURPOSE-LED PUBLISHING™

PAPER • OPEN ACCESS

Turbulent/turbulent entrainment in a planar wake

To cite this article: Oliver R.H. Buxton and Jiangang Chen 2026 *J. Phys.: Conf. Ser.* **3173** 012042

View the article online for updates and enhancements.

You may also like

- YZiCS: Unveiling the Quenching History of Cluster Galaxies Using Phase-space Analysis
Jinsu Rhee, Rory Smith, Hoseung Choi et al.
- Safety, tolerability and blinding efficiency of non-invasive deep transcranial temporal interference stimulation: first experience from more than 250 sessions
Pierre Vassiliadis, Emma Stiennon, Fabienne Windel et al.
- Systematic review of experimental studies in humans on transcranial temporal interference stimulation
Paria Mansourinezhad, Rob M C Mestrom, Debby C W Klooster et al.

This content was downloaded from IP address 146.179.86.32 on 19/02/2026 at 12:42

Journal of Physics: Conference Series **3173** (2026) 012042 doi:10.1088/1742-6596/3173/1/012042

Turbulent/turbulent entrainment in a planar wake

Oliver R.H. Buxton[1] **and Jiangang Chen**[1,2]

[1]Department of Aeronautics, Imperial College London, London, U.K.
[2]School of Aeronautics, Northwestern Polytechnical University, Xi'an, P.R. China

E-mail: o.buxton@imperial.ac.uk

Abstract. Spatially-evolving turbulent/turbulent interfaces (TTIs), demarcating a turbulent wake from decaying background turbulence, are studied alongside the entrainment behaviour between these two adjacent streams of turbulence. Data is acquired experimentally in which a cylinder is placed downstream of a turbulence-generating grid. Various "flavours'' of background turbulence are generated by varying the type of grid and the grid – cylinder separation. Scalar is seeded into the wake and planar laser induced fluorescence (PLIF) is used to distinguish the wake from the background and hence identify the instantaneous location of the TTI. Simultaneous particle image velocimetry (PIV) measurements are conducted to examine the velocity/vorticity fields. Our results show that similarly to turbulent/non-turbulent interfaces (TNTIs) TTIs manifest as a rapid jump in the enstrophy across a short distance. The presence of background turbulence is shown to potentially enhance the entrainment velocity in the near wake, but it substantially suppresses it in the far wake, with the background turbulence intensity being of greatest significance. This affects the entrainment fluxes of mass, momentum, and kinetic energy into the wake, but these fluxes depend on both the entrainment velocity and the surface area of the TTI over which entrainment takes place, which is quantified through the spatially-evolving fractal dimension of the TTI.

1 Introduction

Turbulent flows grow with streamwise distance through the collective processes known as entrainment. Entrainment yields a flux of mass, but also of other quantities such as momentum, energy, scalar etc. across the interface that demarcates the primary turbulent flow from its background. The physics of the special case of entrainment from an irrotational, non-turbulent background have been studied for many years and the physics of entrainment across a turbulent/non-turbulent interface (TNTI) are reasonably well understood. Given that turbulent flows are rotational, the outermost surface of a TNTI is, by definition, a surface of zero enstrophy ($\frac{1}{2}\omega^2$, where $\boldsymbol{\omega} = \nabla \times \boldsymbol{u}$ is the vorticity). [1] was the first to observe that the only source term in the enstrophy transport equation along the outermost boundary of a TNTI (an iso-surface of

Content from this work may be used under the terms of the Creative Commons Attribution 4.0 licence. Any further distribution of this work must maintain attribution to the author(s) and the title of the work, journal citation and DOI.
Published under licence by IOP Publishing Ltd

$\omega^2 = 0$) is viscous diffusion and hence the entrainment across a TNTI is dominated by small-scale viscous processes. This is a result that has subsequently been confirmed experimentally [2] in the twenty-first century. With the advent of DNS, and high-resolution experimental data, it is now clear that TNTIs manifest as a rapid increase in enstrophy, from zero in the background flow to a plateau value (in a statistical sense) just beneath the outermost surface and therefore across a short distance. Whilst the precise scaling for the TNTI thickness is still up for debate it is $\mathcal{O}(10)\eta$, where η is the Kolmogorov length scale e.g. [3]. An excellent review on the nature of TNTIs, methods for detecting them from numerical data, and turbulent entrainment across TNTIs is available in [4].

In general, however, turbulent flows do not reside in ideal, non-turbulent backgrounds but are instead exposed to background flows that are themselves turbulent. For example, cumulus clouds are exposed to atmospheric turbulence and wind-turbine wakes grow within the (turbulent) atmospheric boundary layer. In these circumstances it is no longer possible to state that the outermost surface of a turbulent/turbulent interface (TTI) is an iso-surface of zero enstrophy since there is rotational (turbulent) flow on both sides of a TTI. This raises questions such as "how does a TTI manifest; is it still a rapid jump in enstrophy or something else?" and "how does the presence of background turbulence affect the entrainment fluxes?". These are the questions we seek to address in this contribution.

Recent years has seen progress made with the observation that TTIs are also enstrophy jumps, but from a non-zero level in the background to a plateau value in the primary turbulent flow [5], however no sensible scaling has yet been found to collapse this jump over different flows in which the "flavour" of the background turbulence varies. The physics of TTIs are also different from TNTIs with a negligible role observed for viscous diffusion in bringing about this enstrophy jump which is, instead, yielded by the inertial vorticity stretching arising from the interaction between strain and rotation in the interfacial layer [6]. In turbulent wakes a spatial evolution of the properties of the TTI, and the entrainment mass flux has been observed. In particular, the entrainment mass flux has been observed to be suppressed, with respect to the mass flux across a TNTI, in the far field [5] but enhanced in the near field [7], where the role of the coherent motions (von Kármán vortices) are at their strongest. Further, the tortuoisty, i.e. the degree of contortion of the TTI, is observed to vary spatially and in response to different flavours of background turbulence [8].

2 Methodology

In this contribution we examine how the fundamentally different physics of TTIs affect the entrainment fluxes of mass, momentum, and kinetic energy in a spatially developing planar turbulent wake produced by a circular cylinder of diameter $d = 10$ mm at a diameter-based Reynolds number of $Re_d = 3,800$ ($U_\infty = 0.38$ m s^{-1}). Combined planar PIV and PLIF experiments were conducted in a hydrodynamics flume as depicted in figure 1a. Note that filters were used for both the PIV and PLIF cameras to ensure that only fluorescence was captured in the PLIF cameras and scattered light, from the incident 527 nm Nd:YLF laser, in the PIV cameras. Fluorescent dye (rhodamine 6G) was released into the wake of the cylinder mounted downstream of a turbulence-generating grid. Previous work has shown that the dye faithfully marks the extent of the wake when no grid is placed upstream such that the TNTI as defined by setting a threshold on the modulus of the gradient of the PLIF signal $|\nabla\phi|$ and the out-of-plane component of vorticity magnitude ω_z^2 coincide with one another. By varying the type of grid (fractal or regular) and the grid - cylinder spacing the cylinder is exposed to different "flavours" of (decaying) freestream turbulence (FST) as characterised by the turbulence intensity/integral length scale $\{k, \mathcal{L}\}$ (see figure 1c), where $k = \mathcal{K}^{1/2}/U_\infty$ with $\mathcal{K}$ being the turbulent kinetic energy computed using two-dimensional velocity information, i.e. that available from the planar PIV experiments. High-resolution experiments were conducted to measure the entrainment velocities/fluxes at five different measurement stations centred on streamwise locations $x/d = \{6.5, 10, 20, 30, 40\}$ to enable observation of the spatial evolution of the entrainment. Note that the coordinate system is a standard Cartesian coordinate system with origin at the centre of the cylinder. To give

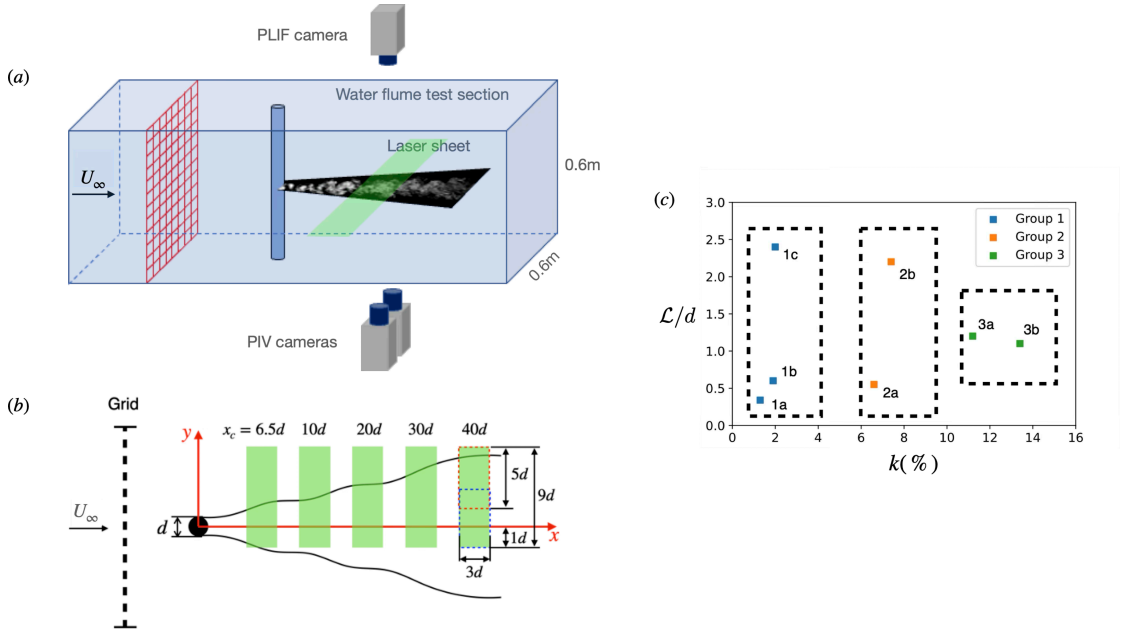


Figure 1: (a) Experimental schematic, (b) location of PIV measurement stations, and (c) parameter space for various "'flavours" (cases) of FST studied.

an indication of the degree of scale separation in the freestream turbulence the Taylor-based Reynolds number in the vicinity of the TTIs at the $x/D = 20$ measurement station ranges from $5 \lesssim Re_\lambda \lesssim 30$ for the mildest flavours (cases 1a and 1b) to $40 \lesssim Re_\lambda \lesssim 60$ for the strongest flavours (cases 3a and 3b), with flavours in group 2 being intermediate. More details on the methodology are provided in [9], including estimates for the spatial resolution which was verified to be sufficient to capture the small-scale dynamics responsible for turbulent entrainment.

3 The manifestation of a turbulent/turbulent interface

3.1 Enstrophy jump

Figure 2 shows ω_z^2, the square of the out-of-plane vorticity component, conditionally averaged on normal distance from the outermost surface of the identified TTI, i.e. $\langle\omega_z^2\rangle(\xi_n)$. Due to the fact that only planar PIV data is available ω_z^2 is used as a surrogate for the enstrophy. Panes (a) and (b) show this conditionally-averaged enstrophy for all measurement stations $x/d \geq 20$ with pane (a) showing cases where the background turbulence is mild (group 1 in figure 1c) and pane (b) showing cases where the background turbulence is intense (group 3 in figure 1c). It can be observed that for all cases the TTI manifests as a jump in enstrophy level, from a lower level in the background to a higher level in the wake itself. In this way the manifestation of a TTI is similar to a TNTI, although presenting the data in the time-averaged sense masks a very important distinction. TNTIs are unidirectional, i.e. there is always a jump from zero enstrophy to a higher level within the primary turbulent flow. Whilst this is also true in the time-averaged sense for a TTI instantaneously this is not true. Preliminary DNS data (not shown here) identified the fact that TTIs contain jumps in which the enstrophy is sometimes (and locally) smaller within the wake than it is in the background, i.e. the TTI is bi-directional. In some senses it is therefore better to interpret a TTI as being a "cliff edge" in the enstrophy field in which sometimes the enstrophy jump is negative, but more often it is positive (in the sense of

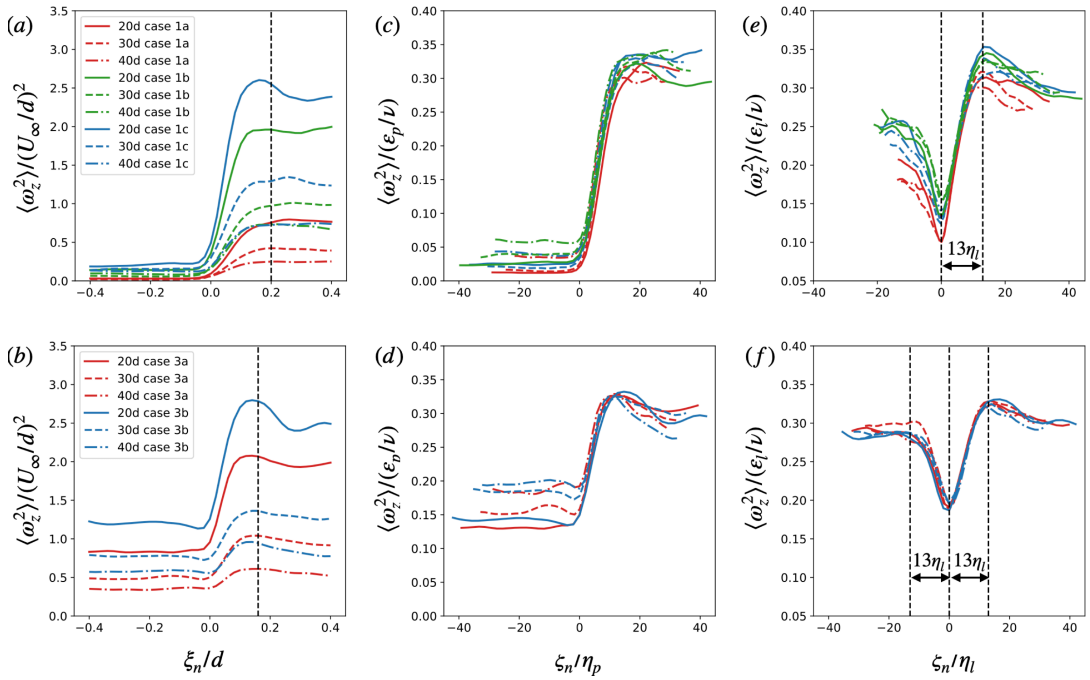


Figure 2: The enstrophy jump across a TTI in low (a, c, e) and high (b, d, f) background turbulence. (a, b) show ω_z^2 normalised by invariant U_∞, d. (c, d) show ω_z^2 normalised by the plateau value of the dissipation rate ε_p at the ξ_n location denoted with the dashed line in (a, b). (e, f) show ω_z^2 normalised by the local ε, i.e. $\varepsilon(\xi_n)$.

$\xi_n > 0$ being within the primary turbulent flow). We aim to report on the local/instantaneous nature of TTIs in future work.

Panes (c) and (d) show the enstrophy jumps associated to the TTIs in mild (group 1) background turbulence (c) and strong (group 3) background turbulence (d) with a normalisation based on the dissipation rate of the turbulence within the wake that is immediately adjacent to the TTI. Observing that the the enstrophy level in the wake attains a plateau value in the region $0.2 \lesssim \xi_n/d \lesssim 0.4$, and noting the result that $\varepsilon = \nu\langle\omega^2\rangle$ for homogeneous turbulence, we define ε_p to be the plateau value of the dissipation rate which is the conditional mean value of the dissipation rate along the black dashed lines of panes (a) and (b). ε_p is thereby representative of the turbulence within the wake immediately adjacent to the TTI and we use this dissipation rate to define a Kolmogorov length scale η_p that is representative of the turbulence on the wake-side of the TTI for normalisation of coordinate ξ_n. $\langle\omega_z^2\rangle$ is normalised by ε_p and the viscosity ν. In comparison to pane (a) we see that this normalisation does a good job of collapsing the curves in pane (c), on both sides of the TTI. Contrastingly, whilst the collapse is reasonable on the wake side of the TTI in pane (d) there is no discernible collapse on the background side of the TTI. This is not surprising given that there are very different varieties of turbulence on both sides of the TTI and a dissipation rate from only one side is used in this normalisation.

A local normalisation, first proposed in [10], is used in panes (e) and (f). The local dissipation rate, $\varepsilon_l(\xi_n)$, is defined as the dissipation rate conditionally averaged as a function of distance normal from the outermost surface of the TTI location, i.e. $\varepsilon_l(\xi_n) \equiv \langle\varepsilon\rangle_{\xi_n}$, more formally, such

that $\varepsilon_l(0)$ corresponds to the dissipation rate averaged along the outermost surface of the TTI, $\xi_n = 0$ etc. The collapse in pane (f) in particular is remarkable when comparing against pane (b). It can be seen that when the background turbulence is intense the TTI consists of two layers. For $\xi_n > 0$ this layer is driven by a rapid increase in the enstrophy, c.f. pane (b). Additional consideration of pane (b) reveals that the layer for $\xi_n < 0$ in pane (f) is clearly not driven by a change in the enstrophy, but is instead driven by the normalisation, i.e. by the local dissipation rate. There are thus two layers adjacent to one another, one dominated by rapid changes in rotation and one dominated by rapid changes in the strain as the turbulence adjusts from being highly inhomogeneous to homogeneous (a value of $\frac{1}{3}$ in this normalisation is indicative of homogeneous turbulence). We finish by observing that both layers are approximately $13\eta_l$ in thickness; a thickness that agrees very well with the proposed high Reynolds number scaling for the turbulent sublayer of a TNTI given by [3].

3.2 Fractal dimension of the turbulent/turbulent interface

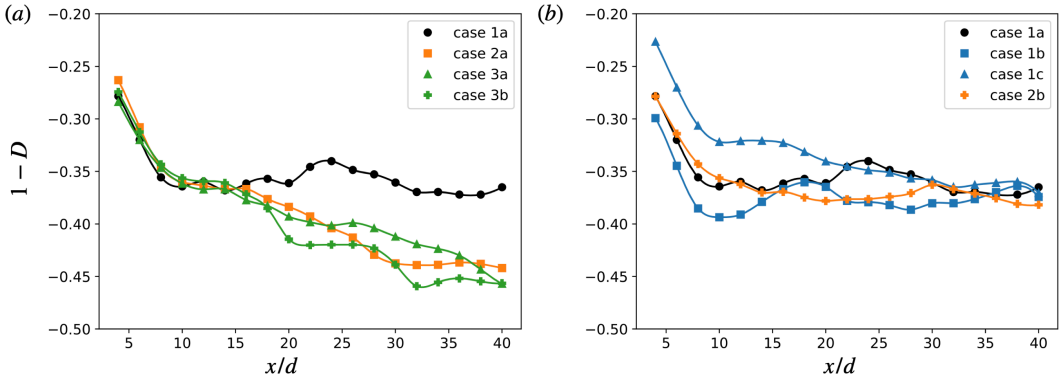


Figure 3: Spatial evolution of $1 - D$, where D is the fractal dimension, of the TTIs (and TNTI) showing the effect of (a) turbulence intensity and (b) integral length scale of the background turbulence.

Having determined that TTIs manifest, in a time-averaged sense, as a jump in the enstrophy over a short distance we now seek to examine the contortion/roughness of the interface. This is an important consideration when determining the entrainment fluxes since it is across the surface area of the interface in which entrainment takes place. We quantify this through computing the fractal dimension of the interface, which has been shown to describe the multi-scale self-similar geometric features of a turbulent interface [11]. The fractal dimension of the interface is computed based off just the PLIF data using the filtering method in which the length of the interface over a particular streamwise extent is computed as a function of increasing filter size. When plotting the logarithm of the interface length, L_I, against the logarithm of the filter size, Δ_f, a straight line can be fitted through a particular range of Δ_f, typically when the filter size is in the inertial range of the turbulent cascade. This slope can then be related to the fractal dimension extracted through $1 - D$, where D is the fractal dimension. More details are provided in [8], including our estimate for the uncertainty in D which is ± 0.02.

Figure 3 shows $1-D$ for some exemplar flavours of background turbulence selected to show the influence of the background turbulence intensity in pane (a) and the integral length scale in pane (b). It can be seen that in the far wake the background turbulence intensity has the largest effect with all TTIs having a larger fractal dimension than the closest experimental approximation to

a TNTI (case 1a). There is minimal effect of background turbulence intensity on D in the near wake. Conversely, in the near wake it is observed that the integral length scale of the background turbulence plays the greatest role in determining D, with the TNTI case 1a being sandwiched between various TTIs yielded by various flavours of background turbulence. In the far wake the integral length scale seems to play a negligible role in determining D.

4 Entrainment across a turbulent/turbulent interface

4.1 Entrainment velocity

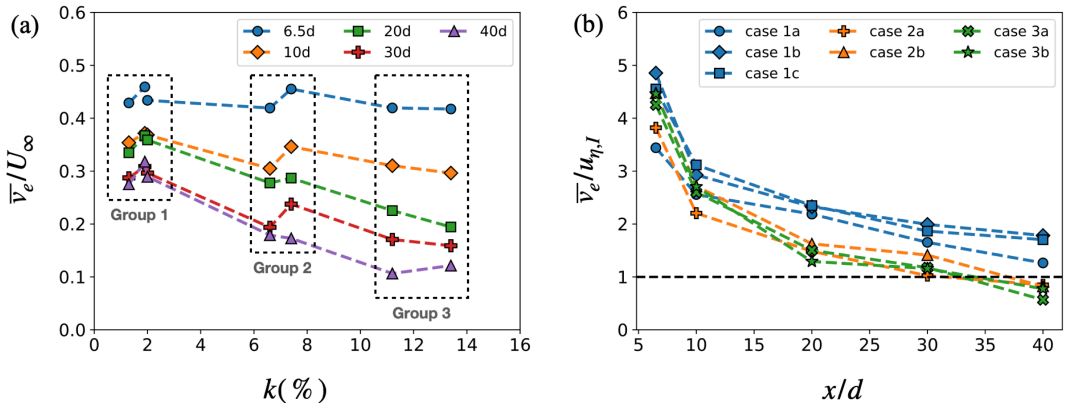


Figure 4: Evolution of the entrainment velocity spatially and with difference cases of FST. (a) normalised by the invariant U_∞, (b) normalised by the local Kolmogorov velocity scale.

We now consider the effect of background turbulence on the entrainment characteristics. Firstly we consider the entrainment velocity; the relative velocity between the motion of the outermost surface of the TTI and the local fluid. At each measurement station, and for each flavour of background turbulence, we compute a mean entrainment velocity $\overline{v}_e$. This is plotted as a function of the turbulence intensity of the background turbulence in figure 4. Focusing on pane (a), which shows $\overline{v}_e$ normalised by the invariant mean velocity U_∞ we make the following observations. Firstly, at all measurement stations, and for all flavours of background turbulence, we see that the mean entrainment velocity decreases with downstream distance. Secondly, we notice a very strong effect of background turbulence intensity on the entrainment velocity at the furthest downstream measurement stations, $x/d \geq 20$, in particular at the farthest downstream measurement station of $x/d = 40$. There is a clear trend that increasing the intensity of the background turbulence suppresses the mean entrainment velocity; there is a roughly threefold reduction in $\overline{v}_e$ between the cases with the lowest background turbulence intensity and those with the highest background turbulence intensity. This is not the case in the farthest upstream measurement station, $x/d = 6.5$, where in many cases $\overline{v}_e$ is slightly larger for cases with moderate background turbulence intensity in comparison to the closest experimental approximation that we have to a TNTI. This result is in keeping with previous results showing that background turbulence can enhance entrainment in the near wake whilst suppressing it in the far wake [7, 5].

Pane(b) shows $\overline{v}_e$ normalised by the local Kolmogorov velocity scale $u_{\eta,l}$, computed from $\varepsilon_l(\xi_n = 0)$. It can be seen that for all flavours of background turbulence $\overline{v}_e/u_{\eta_l}$ decreases and appears to be heading towards a value of $\mathcal{O}(1)$. In any case, whilst it is inappropriate to describe the data as "collapsed" there is nevertheless a much closer agreement between the various flavours of background turbulence and streamwise measurement stations in pane (b) than there is in

pane (a). This perhaps, therefore, offers an explanation for the decrease in $\overline{v}_e$ with streamwise distance since the value of $\overline{v}_e$ seems to align itself somewhat with the local Kolmogorov velocity scale which diminishes with downstream turbulence as the wake/background turbulence decays. This is another avenue for our future research.

4.2 Entrainment fluxes

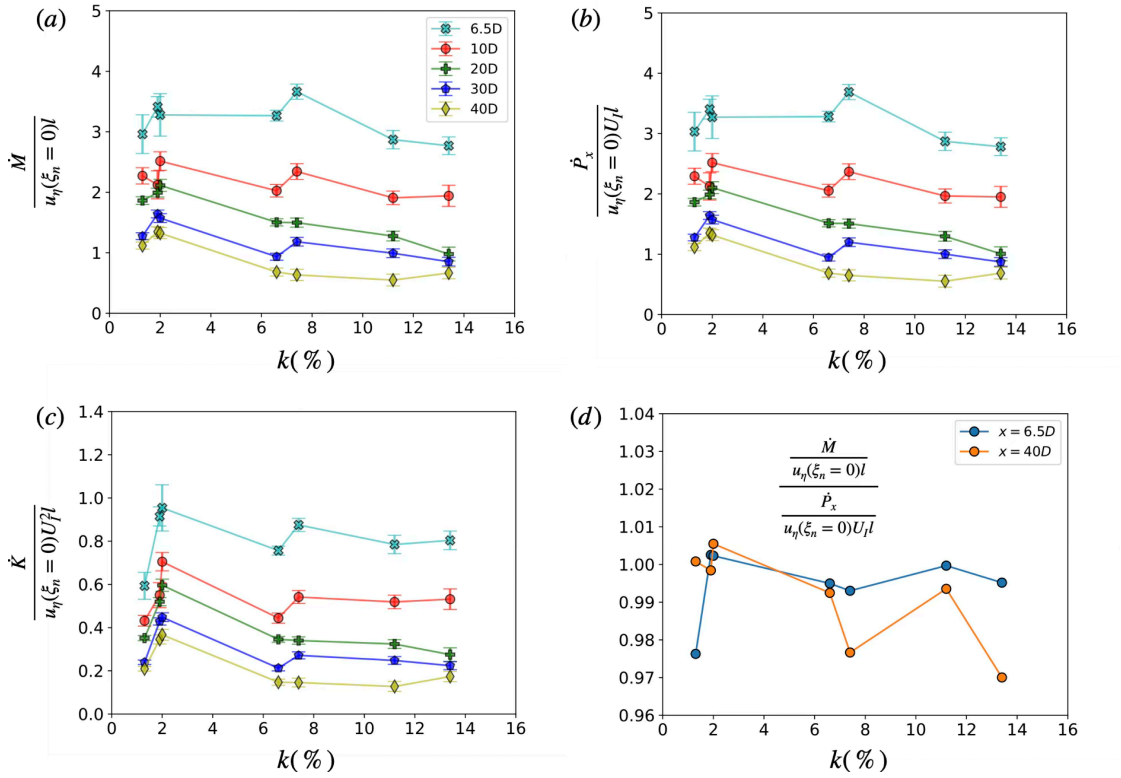


Figure 5: Entrainment fluxes of (a) mass, (b) streamwise momentum, and (c) kinetic energy averaged over the various measurement stations, plotted as a function of intensity of the background turbulence. (d) the ratio of the entrained mass flux to the entrained momentum flux at $x/d \in \{6.5, 40\}$.

When considering a PIV field-of-view of streamwise extent L the entrained mass flux (in two dimensions), $\dot{M}$, is given by

$$\dot{M} = \frac{1}{T}\int_0^T \left(\int_{\ell'(t)} \rho v_e(\xi_s) \mathrm{d}\xi_s \right) \mathrm{d}t =: \overline{\int_{\ell'} \rho v_e \mathrm{d}\xi_s} \tag{1}$$

where ℓ' is the (time-varying) instantaneous length of the interface within the streamwise domain of extent L and the integration is performed along the interface-parallel coordinate ξ_s for $\xi_n = 0$. Similarly, the entrained streamwise momentum flux, $\dot{P}_x$, and kinetic energy flux, $\dot{K}$, are given

by

$$\dot{P}_x = \overline{\int_{\ell'} \rho U v_e \mathrm{d}\xi_s} \tag{2}$$

$$\dot{K} = \frac{1}{2}\overline{\int_{\ell'} \rho \left(U^2 + V^2\right) v_e \mathrm{d}\xi_s} \tag{3}$$

where U and V are the streamwise and cross-stream velocity along the outermost surface of the interface $\xi_n = 0$. Consideration of equations (1)-(3) reveals that the entrainment fluxes are high if, i) the entrainment velocity is large, ii) the interface is sufficiently contorted, i.e. ℓ' is large yielding a large surface area over which the entrainment takes place, and iii) (for the momentum and kinetic energy fluxes) there is a strong correlation between the entrainment velocity and the local fluid velocity (U, V).

Figure 5 shows the three entrainment fluxes, $\dot{M}$ in pane (a), $\dot{P}_x$ in pane (b), and $\dot{K}$ in pane (c) at the various measurement stations and plotted as a function of the intensity of the background turbulence. Considering the mass flux in pane (a) it can be seen that similar trends are observed for the mass flux as for the entrainment velocity in figure 4; $\dot{M}$ decreases with downstream distance, there is a (small) enhancement of entrainment in the near wake, and a suppression of entrainment in the far wake. The suppression of entrainment in the far wake with increasing background turbulence intensity is less pronounced in figure 5 than it is in figure 4, whereas contrastingly the enhancement of entrainment in the near wake with increasing background turbulence intensity is more pronounced. This illustrates the importance of the fact that background turbulence makes TTIs more contorted (see the increased fractal dimension of TTIs in figure 3a), which is an effect that leads to enhanced entrainment fluxes. In the far wake elevated background turbulence intensity additionally suppresses the entrainment velocity, i.e. these two observations work to oppose one another and therefore variation in entrainment flux from the cases with the lowest background turbulence intensity to the highest are less pronounced than the changes in the entrainment velocity. Contrastingly, in the near wake background turbulence can marginally enhance $\overline{v}_e$ whilst also increasing the TTI's surface area and so both effects work together making the differences in the entrainment fluxes more pronounced than those in the entrainment velocity as the background turbulence intensity is increased. It should be noted, however, that the situation is far more complicated in the near wake with some flavours of background turbulence slightly enhancing $\overline{v}_e$ whilst simultaneously both enhancing and decreasing the fractal dimension D of the interface yielding a highly non-linear response for the entrainment fluxes.

Panes (b) and (c) show the entrained streamwise momentum and kinetic energy fluxes, respectively. Quantitatively, the normalised momentum fluxes almost exactly mirror the normalised mass fluxes due to the fact that the momentum flux has been observed to be "slaved" to the mass flux [12]. This is reinforced in pane (d) which shows the ratio $\dot{M}/\dot{P}_x$ at the farthest upstream $(x/d = 6.5)$ and downstream $(x/d = 40)$ measurement stations. This ratio remains extremely close to unity for all flavours of background turbulence and at both measurements stations, reinforcing the fact that the entrained momentum flux is slaved to the mass flux. However, the kinetic energy fluxes in pane (c) are observed to behave similarly, but slightly differently from the mass flux, especially in the measurement stations closest to the cylinder. This is because (small) correlations exist between v_e and (U, V) which enhance the "efficiency" with which kinetic energy is entrained into the wake with respect to the mass [12]. These differences are particularly stark when comparing the case with the lowest background turbulence intensity, our closest experimental approximation to a TNTI, to the remaining TTI cases.

5 Conclusions

Combined PIV and PLIF experiments were conducted in the wake of a circular cylinder exposed to different flavours of decaying background turbulence, characterised by their turbulence

intensities and integral length scales. The instantaneous location of the turbulent/turbulent interface, demarcating the wake from the background was determined using the PLIF data and the neighbouring velocity/vorticity field analysed using the PIV data.

In a time-averaged sense it was shown that the TTI manifests as a jump in enstrophy over a short distance from a lower level in the background to a higher level within the wake. In this sense there is a similarity between a TNTI and TTIs, although the background enstrophy level in a TTI is non-zero. Our experimental work, over a number of years, shows that the most significant parameter that determines the magnitude of this enstrophy jump is the difference in turbulence intensity levels between the background turbulence and the turbulence within the wake. More recent, numerical work [13], has highlighted (unsurprisingly) that a large difference in the r.m.s. enstrophy fluctuation between the two adjacent streams of turbulence forming a TTI also drives a high-magnitude enstrophy jump, but this is difficult to control experimentally.

When normalised by the local Kolmogorov length/velocity scales it is clear that TTIs in which there is intense background turbulence in fact consist of two layers in which the turbulence is highly inhomogeneous. The layer on the wake side is driven by the enstrophy jump but the layer on the background side is driven by the local strain-rate adjusting from an inhomogeneous state to a homogeneous one. The thickness of the two layers was shown to be similar; approximately 13 local Kolmogorov length scales.

The presence of background turbulence was also found to increase the fractal dimension of TTIs, particularly in the far wake. This yields a larger surface area over which entrainment can take place. However, in the far wake it was shown that the presence of background turbulence acts to suppress the mean entrainment velocity, with up to a threefold decrease in $\overline{v}_e$ between the highest and lowest background turbulence intensities studied. These two effects act to oppose one another such that the disparity between the entrainment fluxes between the highest and lowest background turbulence intensities are not as pronounced as those for $\overline{v}_e$. Nevertheless it is still clear that the presence of background turbulence suppresses entrainment across TTIs in comparison to entrainment across TNTIs.

The picture is more complicated in the near wake. The integral length scale plays an important role in determining the fractal dimension of the TTI, and in some cases D can be enhanced with respect to a TNTI whereas in some cases it is reduced. Some cases of background turbulence can marginally enhance the mean entrainment velocity as well such that the picture for the entrainment fluxes is mixed. Cases of moderate background turbulence intensity increase the entrainment fluxes of mass and momentum, whereas the cases with the highest background turbulence intensity make a negligible difference to the entrained mass/momentum fluxes. This is not the case, however, for the entrained kinetic energy flux in which all flavours of background turbulence enhance the entrainment rate with respect to a TNTI. This results from correlations that exist between the entrainment velocity and the local velocity along the outermost surface of the TTI.

References

[1] S. Corrsin and A. L. Kistler. Free-stream boundaries of turbulent flows. *NACA technical report*, (1244), 1955.

[2] J. Westerweel, C. Fukushima, J. Pedersen, and J. C. R. Hunt. Mechanics of the turbulent - non-turbulent interface of a jet. *Physical Review Letters*, 95(17):1–4, 2005.

[3] T. S. Silva, M. Zecchetto, and C. B. da Silva. The scaling of the turbulent/non-turbulent interface at high Reynolds numbers. *Journal of Fluid Mechanics*, 843:156–179, 2018.

[4] C. B. da Silva, J. C. R. Hunt, I. Eames, and J. Westerweel. Interfacial layers between regions of different turbulence intensity. *Annual Review of Fluid Mechanics*, 46(1):567–590, 2014.

[5] K. S. Kankanwadi and O. R. H. Buxton. Turbulent entrainment into a cylinder wake from a turbulent background. *Journal of Fluid Mechanics*, 905:A35, 2020.

[6] K. S. Kankanwadi and O. R. H. Buxton. On the physical nature of the turbulent/turbulent interface. *Journal of Fluid Mechanics*, 942:A31, 2022.

[7] K. S. Kankanwadi and O. R. H. Buxton. Influence of freestream turbulence on the near-field growth of a turbulent cylinder wake: Turbulent entrainment and wake meandering. *Physical Review Fluids*, 8(3):034603, 2023.

[8] J. Chen and O. R. H. Buxton. Spatial evolution of the turbulent/turbulent interface geometry in a cylinder wake. *Journal of Fluid Mechanics*, 969:A4, 2023.

[9] J. Chen and O. R. H. Buxton. Turbulent/turbulent entrainment in a planar wake. *Journal of Fluid Mechanics*, 1000:A26, 2024.

[10] M. Zecchetto and C. B. da Silva. Universality of small-scale motions within the turbulent/non-turbulent interface layer. *Journal of Fluid Mechanics*, 916:A9, 2021.

[11] K. R. Sreenivasan and C. J. F. M. Meneveau. The fractal facets of turbulence. *Journal of Fluid Mechanics*, 173:357–386, 1986.

[12] O. R. H. Buxton and J. Chen. The relative efficiencies of the entrainment of mass, momentum and kinetic energy from a turbulent background. *Journal of Fluid Mechanics*, 977:R2, 2023.

[13] P. D. Alves, M. Zecchetto, R. P. Xavier, O. R. H. Buxton, and C. B. da Silva. Universal features of turbulent/non-turbulent and turbulent/turbulent interfaces. In Jinjun Wang and Ivan Marusic, editors, *Proceedings of the IUTAM Symposium on Turbulent/Non-Turbulent Interface in Turbulent Shear Flows*, pages 94–109. Springer Nature Switzerland, 2025.